

Published in final edited form as:

Cell. 2010 January 8; 140(1): 74–87. doi:10.1016/j.cell.2009.12.011.

Human *TUBB3* mutations perturb microtubule dynamics, kinesin interactions, and axon guidance

Max A. Tischfield^{1,2,3,4,9}, Hagit N. Baris^{3,5,12,56}, Chen Wu^{1,2,9,56}, Guenther Rudolph¹⁵, Lionel Van Maldergem¹⁶, Wei He^{1,2,3}, Wai-Man Chan^{1,2,3,17}, Caroline Andrews^{1,2,3,17}, Joseph L. Demer^{18,19,20,21}, Richard L. Robertson⁸, David A. Mackey^{22,23}, Jonathan B. Ruddle²², Thomas D. Bird^{24,25}, Irene Gottlob²⁶, Christina Pieh²⁷, Elias I. Traboulsi²⁸, Scott L. Pomeroy^{1,2,9,11}, David G. Hunter⁷, Janet S. Soul^{1,11}, Anna Newlin²⁹, Louise J. Sabo³⁰, Edward J. Doherty³¹, Clara E. de Uzcátegui³², Nicolas de Uzcátegui³³, Mary Louise Z. Collins³⁴, Emin C. Sener³⁵, Bettina Wabbels³⁶, Heide Hellebrand³⁷, Thomas Meitinger^{38,39}, Teresa de Berardinis⁴⁰, Adriano Magli⁴⁰, Costantino Schiavi⁴¹, Marco Pastore-Trossello⁴², Feray Koc⁴³, Agnes M. Wong⁴⁴, Alex V. Levin⁴⁵, Michael T. Geraghty⁴⁶, Maria Descartes⁴⁷, Maree Flaherty⁴⁸, Robyn V. Jamieson^{49,50}, H. U. Møller⁵¹, Ingo Meuthen⁵², David F. Callen⁵³, Janet Kerwin⁵⁴, Susan Lindsay^{54,55}, Alfons Meindl³⁷, Mohan L. Gupta Jr.^{10,13,14,*}, David Pellman^{6,10,13}, and Elizabeth C. Engle^{1,2,3,4,5,7,9,11,17,*}

¹Department of Neurology, Children's Hospital Boston, Boston, MA 02115 USA

²FM Kirby Neurobiology Center, Children's Hospital Boston, Boston, MA 02115 USA

³Program in Genomics, Children's Hospital Boston, Boston, MA 02115 USA

⁴The Manton Center for Orphan Disease Research, Children's Hospital Boston, Boston, MA 02115 USA

⁵Department of Medicine (Genetics), Children's Hospital Boston, Boston, MA 02115 USA

⁶Division of Hematology/Oncology, Children's Hospital Boston, Boston, MA 02115 USA

⁷Department of Ophthalmology, Children's Hospital Boston, Boston, MA 02115 USA

⁸Department of Radiology, Children's Hospital Boston, Boston, MA 02115 USA

⁹Program in Neuroscience, Harvard Medical School, Boston, MA 02115, USA

¹⁰Division of Hematology/Oncology, Harvard Medical School, Boston, MA 02115, USA

¹¹Department of Neurology, Harvard Medical School, Boston, MA 02115, USA

¹³Department of Pediatric Oncology, Dana-Farber Cancer Institute, Boston, MA 02115, USA

© 2011 Published by Elsevier Inc.

*Corresponding authors: Elizabeth C Engle MD, CLS14074, Children's Hospital Boston, 300 Longwood Ave, Boston, MA 02115. Tel. 617-919-4030. Elizabeth.Engle@childrens.harvard.edu. Mohan Gupta PhD, Department of Molecular Genetics and Cell Biology, The University of Chicago, Chicago, Illinois 60637. mlgupta@uchicago.edu.

¹²Current affiliation: The Raphael Recanati Genetic Institute, Rabin Medical Center, Beilinson Hospital, Petach-Tikva, Israel

¹⁴Current affiliation: Department of Molecular Genetics and Cell Biology, The University of Chicago, Chicago, Illinois 60637

⁵⁶These authors contributed equally to this work.

Supplemental Text

Supplemental Text includes 6 figures, 3 tables, 3 movies, and supplemental experimental procedures, and references and can be found with the article online at <http://cell.com/supplemental/X>.

Publisher's Disclaimer: This is a PDF file of an unedited manuscript that has been accepted for publication. As a service to our customers we are providing this early version of the manuscript. The manuscript will undergo copyediting, typesetting, and review of the resulting proof before it is published in its final citable form. Please note that during the production process errors may be discovered which could affect the content, and all legal disclaimers that apply to the journal pertain.

- ¹⁵University Eye Hospital, Ludwig-Maximilians-University, Munich, Germany
- ¹⁶Centre de génétique humaine Université de Liège, Domaine universitaire du Sart-Tilman, B-4000 Liège, Belgium
- ¹⁷Howard Hughes Medical Institute, Chevy Chase, MD 20815, USA
- ¹⁸Department of Ophthalmology and Jules Stein Eye Institute, David Geffen Medical School at University of California Los Angeles
- ¹⁹Department of Neurology, David Geffen Medical School at University of California Los Angeles
- ²⁰Neuroscience Interdepartmental Program, David Geffen Medical School at University of California Los Angeles
- ²¹Bioengineering Interdepartmental Program, David Geffen Medical School at University of California Los Angeles
- ²²Centre for Eye Research Australia, Department of Ophthalmology, University of Melbourne, Royal Victorian Eye and Ear Hospital, East Melbourne, Victoria, 3002, Australia
- ²³Department of Ophthalmology, Royal Hobart Hospital, University of Tasmania, Hobart Tasmania, 7000, Australia
- ²⁴Department of Neurology and the Department of Medicine, University of Washington School of Medicine, Seattle, WA 98195, USA
- ²⁵GRECC, VA Puget Sound Health Care System, Seattle, WA
- ²⁶Ophthalmology Group, University of Leicester, Leicester, LE2 7LX, UK
- ²⁷University Eye Hospital, University of Freiburg, Killianstr. 6, 79106 Freiburg, Germany
- ²⁸Cole Eye Institute, Cleveland Clinic i32, 9500 Euclid Avenue Cleveland, OH 44195
- ²⁹Center for Medical Genetics, NorthShore University HealthSystem, Evanston, IL 60201
- ³⁰Department of Ophthalmology, Geisinger Medical Institute, Danville, Pennsylvania
- ³¹Atlantic Health Science Centre, Saint John Regional Hospital, Saint John New Brunswick, Canada
- ³²Instituto de Oftalmologia, Av. Cajigal 48. Piso 3 Consultorio 8. San Bernardino, Caracas 1010 Venezuela
- ³³Department of Ophthalmology, Upstate Medical University SUNY. Eye Consultants Of Syracuse, 1101 Erie Blvd. East Ste 100. Syracuse NY 13210
- ³⁴Department of Ophthalmology, Greater Baltimore Medical Center Baltimore, MD 21204
- ³⁵Department of Ophthalmology, Hacettepe University Hospitals, Ankara 06100, Turkey
- ³⁶Department of Ophthalmology, University of Bonn, Abbestr. 2, D-53127, Bonn, Germany
- ³⁷Department of Obstetrics and Gynaecology, Klinikum rechts der Isar, Technische Universität München, Ismaningerstr 22, 81675 Munich, Germany
- ³⁸Institute of Human Genetics, Klinikum rechts der Isar, Technische Universität München, Ismaningerstr 22, 81675 Munich, Germany
- ³⁹Institute of Human Genetics, Helmholtz Zentrum München, Ingolstädter Landstr. 1, 85764 Neuherberg, Germany
- ⁴⁰Department of Ophthalmologic Sciences, Faculty of Medicine and Surgery, University "Federico II", Naples, Italy

⁴¹Department of Ophthalmology, University of Bologna, Bologna, Italy

⁴²Department of Neuro-Radiology, S.Orsola-Malpighi Hospital via Albertoni, 15, 40138, Bologna, Italy

⁴³Department of Ophthalmology and Strabismus, and Neuroophthalmology, Acibadem University Kocaeli Hospital, Kocaeli 41100 Turkey

⁴⁴Department of Ophthalmology and Vision Sciences, The Hospital for Sick Children, Toronto, Ontario Canada

⁴⁵Pediatric Ophthalmology and Ocular Genetics, Wills Eye Institute, Philadelphia, PA

⁴⁶Department of Genetics, Children's Hospital Eastern Ontario, Canada

⁴⁷Department of Genetics, University of Alabama at Birmingham, Birmingham, Alabama

⁴⁸Department of Ophthalmology, The Children's Hospital at Westmead, Sydney, Australia

⁴⁹Department of Clinical Genetics, The Children's Hospital at Westmead, Sydney, Australia

⁵⁰The University of Sydney, Sydney, Australia

⁵¹Department of Ophthalmology, Viborg Hospital, DK 8000 Viborg Denmark

⁵²Department of Hematology-Oncology, Kliniken der Stadt Köln, Neufelderstr. 32, 51067 Köln, Germany

⁵³Breast Cancer Genetics Group, School of Medicine, University of Adelaide, Australia

⁵⁴Institute of Human Genetics, Newcastle University, Newcastle upon Tyne NE1 3BZ, UK

⁵⁵MRC-Wellcome Trust Human Developmental Biology Resource (Newcastle), Newcastle University, Newcastle upon Tyne NE1 3BZ, UK

Abstract

We report that eight heterozygous missense mutations in *TUBB3*, encoding the neuron-specific β -tubulin isotype III, result in a spectrum of human nervous system disorders we now call the *TUBB3* syndromes. Each mutation causes the ocular motility disorder CFEOM3, whereas some also result in intellectual and behavioral impairments, facial paralysis, and/or later-onset axonal sensorimotor polyneuropathy. Neuroimaging reveals a spectrum of abnormalities including hypoplasia of oculomotor nerves, and dysgenesis of the corpus callosum, anterior commissure, and corticospinal tracts. A knock-in disease mouse model reveals axon guidance defects without evidence of cortical cell migration abnormalities. We show the disease-associated mutations can impair tubulin heterodimer formation *in vitro*, although folded mutant heterodimers can still polymerize into microtubules. Modeling each mutation in yeast tubulin demonstrates that all alter dynamic instability whereas a subset disrupts the interaction of microtubules with kinesin motors. These findings demonstrate normal *TUBB3* is required for axon guidance and maintenance in mammals.

Introduction

Nervous system development is highly dependent upon the microtubule cytoskeleton. Microtubules are copolymers assembled from tubulin heterodimers, which contain several different α - and β -tubulin isotypes encoded by separate genes (Lopata and Cleveland, 1987). Microtubule behavior varies according to isotype composition, suggesting each isotype may have properties necessary for specific cellular functions (Joshi and Cleveland, 1990; Luduena, 1993); however, precise functions for most tubulin isotypes remain poorly

characterized. β -tubulin isotype III (TUBB3), one of at least six β -tubulins found in mammals, is distinct because purified microtubules enriched in TUBB3 are considerably more dynamic than those composed from other β -tubulin isotypes (Panda et al., 1994), and because its expression is primarily limited to neurons (Katsetos et al., 2003). *TUBB3* expression is greatest during periods of axon guidance and maturation; levels decrease in the adult central nervous system (CNS) but remain high in the peripheral nervous system (PNS) (Jiang and Oblinger, 1992). Thus, the unique dynamic properties and spatio-temporal expression pattern of TUBB3 suggest it could have a specific function for nervous system development and axon maintenance.

The development of human brainstem ocular motor neurons is particularly vulnerable to gene mutations that affect cytoskeletal proteins and axon guidance (Miyake et al., 2008; Yamada et al., 2003). Congenital fibrosis of the extraocular muscles type 3 (CFEOM3) is a rare ocular motility disorder in which affected individuals are born with blepharoptosis (drooping eyelids) and restricted eye movements (Doherty et al., 1999; Mackey et al., 2002). Using CFEOM3 as a marker for gene mutations that regulate human nervous system development and function, we now report that 8 different heterozygous missense mutations in *TUBB3*, also known as TuJ1, result in CFEOM3 in isolation or as a component of several previously undefined neurological syndromes. Neuroradiological and pathological findings in humans and a knock-in mouse model, respectively, demonstrate that TUBB3 is necessary for guidance of commissural fibers and cranial nerves. Furthermore, disease-associated mutations can alter microtubule dynamics, and a subset perturbs the interaction of microtubules with kinesin motor proteins. Thus, our work to define the TUBB3 syndromes establishes the requirement for a neuronal β -tubulin isotype in axon guidance and normal brain development.

Results

Eight heterozygous *TUBB3* mutations alter six amino acid residues

CFEOM3 in the absence of additional neurological signs or symptoms ('isolated CFEOM3') is a ~90% penetrant autosomal dominant disorder that had previously been mapped to chromosome 16q in pedigrees BN and DP (OMIM#600638, Figure S1A, Table S1A, B) (Doherty et al., 1999; Mackey et al., 2002). The critical region for the CFEOM3 gene was 3.5 Mb and flanked by D16S498-16qter. To identify the CFEOM3 gene, we screened coding exons and intron-exon boundaries of positional candidates in probands from BN, DP, and additional families with isolated CFEOM3. We identified three heterozygous *TUBB3* missense changes in 15 unrelated pedigrees: 784C>T (R262C) in 11 pedigrees, 904G>A (A302T) in three pedigrees, and 185G>A (R62Q) in one pedigree (Figure S1B, Table S1B, C, D).

We had ascertained study participants with CFEOM and additional neurological symptoms and, given the pan-neuronal expression of TUBB3 in humans (<http://www.hudsen.org>, HUDSEN Human Gene Expression Spatial Database, ID: 411), we next sequenced DNA from these probands. We identified five additional heterozygous *TUBB3* missense changes in 13 unrelated pedigrees. 1249G>C (D417H) and 1249G>A (D417N) alter the same residue and co-segregate in a dominant fashion in one and four pedigrees, respectively. The remaining mutations, 1138C>T (R380C), 785G>A (R262H), and 1228G>A (E410K), were found in one, two, and six pedigrees, respectively, and each arose *de novo* as sporadic disease or from presumed germ-line mosaicism (Figure S1B, Table S1A, E). Each of the eight mutations segregated with the TUBB3 phenotype, was absent in parents of sporadic individuals, and was not present on over 1700 control chromosomes. The independent nature of the recurrent mutations is supported by *de novo* occurrences, ethnic and

geographic diversity among probands, and multiple disease-associated haplotypes (Table S1C).

***TUBB3* mutations can result in congenital oculomotor nerve hypoplasia and later-onset peripheral axon degeneration**

Congenital ocular motility defects resulting from R262C, A302T, R380C, and D417N amino acid substitutions ranged from mild to severe (Figure 1A–E), as previously described for pedigree BN (Doherty et al., 1999), whereas all participants with R262H, E410K, and D417H had severe CFEOM3 and congenital facial weakness (Figure 1G, H). Many subjects had aberrant eye movements and several had ptotic eyelid elevation associated with synkinetic jaw movements (Marcus Gunn phenomenon), clinical manifestations of aberrant innervation of cranial musculature by the trigeminal nerve. We conducted magnetic resonance imaging (MRI) of the intracranial motor nerves and orbital contents of affected members of four R262C or D417N pedigrees. Similar to imaging of individuals with *KIF21A* missense mutations which cause the isolated oculomotility disorder, CFEOM1 (Demer et al., 2005), we found hypoplasia of the oculomotor nerve and the muscles innervated by its superior division - the levator palpebrae superioris and superior rectus - as well as the medial rectus muscle innervated by its inferior division (Figures 1J–L, S1C). The oculomotor nerve also aberrantly innervated the lateral rectus muscle, normally innervated by the abducens nerve. Thus, ocular motility restrictions and/or synkinetic lid elevation with jaw movements could be explained by axon guidance defects.

All subjects harboring D417H or R262H were born with congenital wrist and finger contractures, suggesting maldevelopment of spinal motor neurons (Figure 1I), and developed lower extremity weakness and sensory loss in the first decade of life. Most subjects harboring D417N and the oldest patient harboring E410K developed lower extremity weakness and sensory loss in the second to third decade, all in the absence of congenital contractures (Figure 1F). Electromyography revealed chronic, generalized sensorimotor polyneuropathy that was predominantly axonal, and diagnosed as Charcot-Marie-Tooth Type 2 (CMT2) in some subjects. Several participants harboring D417N without CFEOM3 developed polyneuropathy (Table S1E), suggesting that *TUBB3* mutations can cause an isolated CMT2-like disorder.

***TUBB3* mutations can result in commissural axon and basal ganglia malformations that segregate with developmental disabilities**

Brain imaging was reviewed from individuals with each *TUBB3* mutation except D417H, and appeared normal only in the R62Q subject. Common findings were dysgenesis of the corpus callosum (CC), anterior commissure (AC), and internal capsule; generalized loss of white matter; and basal ganglia dysmorphisms that correlated with specific mutations (Figure 2). No images showed cortical dysplasia or evidence of cortical migration defects. Intellectual and behavioral impairments generally correlated with the severity of CC dysgenesis. Individuals with A302T, E410K, R262H, and R380C had more severe CC dysgenesis and mild to moderate intellectual, social, and behavioral impairments. By contrast, those with R62Q, R262C, or D417N substitutions had absent or mild CC dysgenesis and most were developmentally normal (Table S1).

R262C *Tubb3* substitution results in impaired axon guidance but normal cortical architecture in mice

To further examine the nature of the nervous system defects in humans, we generated a disease mouse model harboring the most common amino acid substitution (R262C) (Figure S2A). Wild-type (WT) and *Tubb3*^{+/R262C} mice were born at the expected Mendelian frequencies; heterozygous mice appeared healthy, did not display external eye phenotypes,

and had histologically normal appearing brains. Similarly, the R262C phenotype in humans can be non-penetrant, and when penetrant is limited to CFEOM3. By contrast, *Tubb3*^{R262C/R262C} mice failed to breathe normally and died within hours of birth. Overall brain size was similar between WT and *Tubb3*^{R262C/R262C} littermates, although basal ganglia asymmetries were sometimes present.

Histological analysis at E18.5 revealed normal cortical layer thickness and architecture in both homozygous and heterozygous mice versus WT littermates, and neocortical layer-specific markers confirmed that layering was preserved (Figures 3A–H, S2C). The hippocampus and dentate gyrus also appeared normal (Figure S2B). Thus, consistent with human MR findings, heterozygous and homozygous R262C mice do not show evidence of cortical cell migration defects.

Tubb3^{R262C/R262C} mice showed defects in the guidance of commissural axons and cranial nerves. There was significant thinning and/or absent midline crossing of the AC throughout its anterior-posterior axis compared to WT mice; it appeared tortuous and often had aberrant fiber projections at the midline. The AC was also thinner at the midline in *Tubb3*^{+ /R262C} mice, similar to human patients (Figures 3I, K, S2D). Agenesis of the CC with bundles of stalled axons (Probst bundles) adjacent to the midline was observed in 2/5 homozygous mutant mice, both of which were on a mixed C57BL/6J:129S6 background (Figure 3J, L). By contrast, CC morphology was normal in all 18 mixed background WT mice analyzed. In the three homozygous mice in which the CC crossed the midline, it appeared abnormally thin in two and thick in one (Figure 3K). Whole-mount neurofilament staining at E11.5–E12 revealed numerous defects in the guidance and branching of cranial nerves (Figure 3M–P). The oculomotor nerve failed to reach the correct muscle anlage and instead projected toward the position of the superior oblique muscle that is normally innervated by the trochlear nerve. Trochlear nerve growth was often stalled, and the trigeminal nerve failed to grow and branch properly compared to WT littermates. These data strongly support a primary defect in the guidance of axons.

***Tubb3*^{R262C/R262C} mice have increased microtubule stability and decreased Kif21a microtubule interactions**

There was a decrease in the level of TUBB3 protein in *Tubb3*^{R262C/R262C} and *Tubb3*^{+ /R262C} versus WT mice. Although protein levels in homozygous mutant mice were approximately 30% of WT values, remaining mutant protein incorporated into microtubules that were polymerized *in vitro* from brain extracts, as well as into microtubules throughout the cytoskeleton of dissociated cortical and hippocampal neurons (Figure 4A, B, D). Because *Tubb3* is thought to be the most dynamic β -tubulin isotype, we asked if protein loss and/or the remaining mutant protein altered microtubule stability in the brain. We detected an approximate 30% increase in the levels of de-tyrosinated α -tubulin (Figure 4C), a post-translational modification that is indicative of stable microtubules (Webster et al., 1987). We also measured the steady-state level of tubulin polymerization in brain extracts from WT and homozygous mutant littermates. Although overall α -tubulin levels were decreased in *Tubb3*^{R262C/R262C} brain lysates, there was an increase in the amount of tubulin polymerization as detected by a larger microtubule pellet (Figure 4D). Taken together, these data suggest that microtubule stability is increased in *Tubb3*^{R262C/R262C} mutants.

We next asked whether Kif21a microtubule interactions are altered in *Tubb3*^{R262C/R262C} mutants because heterozygous mutations in this kinesin in humans cause isolated ocular motor dysfunction with clinical and neuroradiological signs of cranial nerve axon guidance defects (Demer et al., 2005; Yamada et al., 2003). We analyzed the ability of Kif21a to co-purify with microtubules isolated from the brains of *Tubb3*^{R262C/R262C} mutant and WT littermates in the presence of ATP. A significant decrease of Kif21a was detected with

microtubules from the brains of *Tubb3*^{R262C/R262C} mice (Figure 4E). Thus, reduced *Tubb3* microtubule incorporation and/or the residual mutant protein affect the ability of Kif21a to interact with microtubules and may contribute to oculomotor nerve misguidance in mice and humans. Commissural axon guidance defects and other *TUBB3* disease-specific phenotypes not found in CFEOM1 patients suggest that additional motors and/or MAPs beyond Kif21a may also be affected.

TUBB3 mutants show variable reductions in heterodimer formation but form microtubules in mammalian cells

A series of interactions with protein chaperones fold quasi-native tubulin monomers into functional $\alpha\beta$ -tubulin heterodimers that can then polymerize into microtubules (Lewis et al., 1996). Point mutations in α - and β -tubulin can impair interactions with chaperone proteins, resulting in reduced heterodimer formation in mammalian cells (Jaglin et al., 2009; Keays et al., 2007), and could explain low protein levels observed in mutant mice. Thus, we asked whether R262C and the other seven substitutions affect the formation of *TUBB3* heterodimers.

The coding sequences of WT and all eight *TUBB3* mutants were fused to a C-terminal V5 epitope tag (*TUBB3*-V5) and expressed in rabbit reticulocyte lysate. This lysate is a cell-free system that contains necessary molecular chaperone proteins for *de novo* tubulin heterodimer formation (Cleveland et al., 1978); resulting heterodimers are comprised of rabbit α -tubulin and WT or mutant *TUBB3*-V5. WT and mutant proteins were expressed and translated at equivalent levels. Under native conditions, R62Q, R262C, A302T, and R380C showed significant reductions in heterodimer yield, whereas the remaining four mutants generated moderate yields (Figure 4F). This latter group was mixed with bovine brain tubulin and taken through two successive rounds of microtubule polymerization and depolymerization. The ability of these mutant heterodimers to co-cycle with native tubulin *in vitro* was equivalent to WT (Figure 4G).

WT and mutant *TUBB3*-V5 expression constructs were next transfected into HeLa cells that have well demarcated microtubules. Immunostaining against the C-terminal V5 tag and α -tubulin to detect the overall microtubule network revealed incorporation of WT and mutant heterodimers. Cells expressing R62Q and R262C *TUBB3*, however, had lower and more punctuate microtubule incorporation, whereas A302T, R380C, and the remaining mutants showed robust incorporation that was similar to WT (Figure S3). Interestingly, patients harboring R62Q or R262C have the mildest phenotypes, and this could result from lower amounts of mutant heterodimer incorporation into microtubules compared to the other mutants. Thus, although four disease-associated substitutions show scant heterodimer formation *in vitro*, all of the mutants can be incorporated into microtubules in mammalian cells, albeit at varying levels.

TUBB3 amino acid substitutions are located in different structural domains within β -tubulin

TUBB3-disease substitutions reside in regions of β -tubulin implicated in the regulation of microtubule dynamics, motor protein trafficking, and interactions with microtubule associated proteins (MAPs) (Li et al., 2002; Lowe et al., 2001) (Figure 5A–D, Movie S1). Residues R62 and A302 reside in regions proposed to mediate lateral interactions between longitudinal units of $\alpha\beta$ -tubulin heterodimers, called protofilaments, which assemble to form cylindrical microtubules. Lateral protofilament interactions aid microtubule assembly and regulate dynamics (Nogales and Wang, 2006). By contrast, residues R380, E410, and D417 are found in paired alpha-helices H11 (R380) and H12 (E410, D417) on the external surface of microtubules that mediates interactions with numerous motor proteins and MAPs (Al-

Bassam et al., 2002; Uchimura et al., 2006). Residue R262 is located in the loop between helix H8 and strand 7 of β -tubulin below helix H12, and forms a putative hydrogen bond with H12 through the carbonyl oxygen of residue D417. Upon mutation, this hydrogen bond is abolished, potentially affecting the tertiary protein structure and motor protein interactions with microtubules (Figure 5E).

The locations of the TUBB3 substitutions suggest that some could directly affect lateral protofilament interactions and microtubule dynamics, whereas others may also perturb motor protein interactions. Notably, these substitutions can result in diagnostically distinct phenotypes (Figure 5F), leading us to ask whether they could alter TUBB3 function and cause dominant effects upon microtubule behavior.

Insertion of human *TUBB3* mutations into the yeast -tubulin locus affects cell viability and growth

The sequence and protein structure of β -tubulin is conserved between different isoforms and across species (Ludueno, 1993). TUBB3 shares considerable homology with the single β -tubulin isoform in budding yeast (Tub2p), including conservation of all disease-associated residues (Figure S4). Budding yeast provides advantages for studying the behavior of microtubules harboring TUBB3-disease substitutions (Reijo et al., 1994). Mutations can be introduced into *TUB2* by homologous recombination, and a single β -tubulin isoform avoids the potential diminution of mutant phenotypes due to an abundance of other tubulin isoforms.

To examine potential dominant effects of disease associated mutations, we inserted each into the yeast *TUB2* locus, and two independent heterozygous diploid strains for each mutation were isolated and grown on nutrient rich media. Heterozygous diploids were recovered at the expected frequency and did not display growth defects on rich medium, establishing that all of the mutant heterozygous strains were viable. However, only R62Q and R380C haploid spores were viable when present as the sole copy of *TUB2*, and they grew slowly compared to WT (Table S2).

TUBB3 disease substitutions result in benomyl resistance and alter microtubule dynamics

To determine if mutant substitutions affect microtubule dynamics, WT, heterozygous, and surviving haploid *TUB2* mutant strains were plated on media containing increasing amounts of benomyl, a compound that destabilizes microtubules and consequently inhibits cell division. Control strains grew normally on complete media without benomyl, but were modestly or completely inhibited by increasing drug concentrations. By contrast, all mutant diploid strains demonstrated varying degrees of benomyl resistance compared to WT (Figure S5A, B); this is in contrast to a previously reported *TUB2* mutagenesis screen, in which alterations of conserved residues more often cause benomyl supersensitivity than resistance (Reijo et al., 1994). These results suggest that TUBB3 syndrome mutations in Tub2p increase the stability of microtubules by rendering them resistant to depolymerization. Finally, a heterozygous diploid strain was generated in which one copy of *TUB2* was deleted. Unlike the TUBB3 substitutions, *TUB2* haplo-insufficiency resulted in benomyl sensitivity (Figure S5A, B). Thus, the TUBB3 substitutions do not result in complete loss of *TUB2* function and appear to cause dominant effects on microtubule behavior.

Using time-lapse microscopy, we then asked how TUBB3 syndrome mutations alter microtubule dynamics. We monitored astral microtubules in G1 cells since microtubules are most dynamic during G1 (Carminati and Stearns, 1997). GFP-Tub1p (α -tubulin) labeled microtubules from heterozygous strains R262C, R262H, A302T, and E410K and haploid

strains R62Q and R380C were imaged because these residues reside within different regions of the tubulin dimer.

Substitutions A302T, R62Q, and R380C resulted in similar and significant changes to most measured parameters of microtubule dynamics (Figure 6A–C). Mutant microtubules were more stable and had longer lifetimes compared to WT, and spent the majority of time in prolonged paused states instead of growing and shortening. The frequency of transition to microtubule depolymerization (catastrophe) was reduced, whereas the frequency of transition to polymerization (rescue) was unaffected in A302T heterozygotes, and increased in R62Q and R380C haploids. The rates of both polymerization and depolymerization were significantly reduced. R380C microtubules appeared less dynamic than R62Q and A302T microtubules and spent more time in paused states, although WT tubulin in heterozygous A302T cells might dampen stability. Thus, A302T, R62Q, and R380C substitutions appear to increase the stability of microtubules and significantly diminish overall dynamics (Movie S2). A302 and R62 are found in loops within β -tubulin hypothesized to regulate lateral protofilament interactions and thus might be predicted to alter stability when mutated. In contrast, this finding is somewhat unexpected for R380C, given that this residue resides in H11, and to our knowledge this outer helix has not been previously implicated in the regulation of microtubule dynamics.

Diploid R262C, R262H, and E410K substitutions resulted in changes to dynamics distinct from those described above (Figure 6B, C). Microtubules in these heterozygous cells spent similar amounts of time growing compared to WT, but the average duration of individual growth events was prolonged and astral microtubules in these strains were longer on average (Figure S5C). The frequency of catastrophe events was only slightly less, whereas the frequency of rescue events was significantly less than WT. Finally, these mutants showed a decreased rate of polymerization and increased rate of depolymerization. Thus, mutant R262C, R262H, and E410K astral microtubules were often long and grew at reduced polymerization rates, followed by a more rapid and complete disassembly to the spindle pole body without recovery (Movie S2).

Mutation at amino acid residues E410, D417, and R262 result in a loss of kinesin localization on microtubule plus-ends

Amino acid residues E410 and D417 of yeast β -tubulin have been identified as microtubule binding sites for conventional kinesin (Kif5) *in vitro* (Uchimura et al., 2006), and we predict R262 forms a hydrogen bond with D417, which is abolished by R262C/H substitutions (Figure 5E). Perturbations to microtubule dynamics observed in R262C/H and E410K cells, including the faster rate of depolymerization and reduced rescue frequency, are similar to those found following the deletion of Kip3p (Kip3 Δ). Kip3p is a plus-end directed kinesin motor found in yeast cytoplasm, and is necessary to position the mitotic spindle near the bud neck in dividing cells (DeZwaan et al., 1997). Kip3 Δ , R262C/H, and E410K mutant cells often have long microtubules that result in mispositioning of the mitotic spindle away from the bud neck (Gupta et al., 2006).

Altered dynamic instability resulting from some TUBB3 substitutions might be explained by reduced Kip3p-microtubule interactions. Thus, we monitored the behavior of Kip3p *in vivo* fused to three tandem copies of YFP at its c-terminus (Kip3p-3YFP) in heterozygous mutant and WT cells containing CFP-Tub1p labeled microtubules. Localization of Kip3p-3YFP on WT microtubules was as previously reported, with strong intensity detected on the plus-end tips and discontinuous speckles along the length of cytoplasmic microtubules (Figure 7A, F) (Gupta et al., 2006). Time-lapse video microscopy revealed a strong reduction of Kip3p-3YFP along the lengths and tips of growing microtubules in R262C/H, E410K, and D417H/N cells (Movie S3). Overall, R262C/H, E410K, and D417H/N cells all had a ~70–

80% decrease in signal intensity compared to WT (Figure 7B–J, U). We next examined the plus-end localization of Kip2p-3YFP, as Kip2p is the second major anterograde motor found in the budding yeast cytoplasm. Kip2p-3YFP localization was normal in WT cells; it was absent from spindle pole bodies, and was speckled along the lengths and highly localized to the plus-ends of astral microtubules (Figure 7K, P) (Carvalho et al., 2004). Mutant R262C/H, E410K, and D417H/N cells had a significant, albeit less dramatic and more variable, decrease in Kip2p-3YFP plus-end localization compared to Kip3p (Figure 7L–T, V). There were no significant differences in the protein levels of Kip3p-3YFP and Kip2p-3YFP between WT and mutant cells to account for the quantitative differences (Figure S6). Thus, the R262C, R262H, E410K, D417N, and D417H substitutions result in a significant decrease in Kip3p-3YFP and Kip2p-3YFP accumulation on microtubule plus-ends, suggesting that kinesin interactions on microtubules are reduced in humans harboring these amino acid substitutions. These data provide *in vivo* evidence to support previous *in vitro* studies (Uchimura et al., 2006) implicating E410 and D417, as well as identifying an additional residue, R262, as important amino acids for proper microtubule-kinesin interactions. These findings also support diminished KIF21A microtubule-interactions found in $TUBB3^{R262C/R262C}$ mice.

The localization of Kip3p-3YFP and Kip2p-3YFP on the plus-ends of cytoplasmic microtubules was not significantly altered between WT, R62Q and A302T heterozygous mutant cells (Figure 7U, V), and these residues are distal from known kinesin-microtubule interaction sites. Cytoplasmic microtubules in heterozygous R380C cells had an approximately 50% increase in the amount of Kip3p-3YFP at the plus-ends, but a non-significant increase in the amount of Kip2p-3YFP (Figure 7U, V). Thus, residues R62Q, A302T, and R380C all diminish microtubule dynamics in a similar fashion, and do not significantly reduce the levels of kinesin on the plus ends of microtubules.

Discussion

Phenotype-genotype correlations in the *TUBB3* syndromes support a dominant etiology

We have identified *TUBB3* as the mutated gene underlying a series of autosomal dominant disorders of axon guidance that we collectively call the *TUBB3* syndromes. In 29 unrelated families, we identified eight unique heterozygous missense mutations that alter six amino acid residues. Phenotype-genotype correlations are emerging for these syndromes, and while the *TUBB3* phenotypes limited to CFEOM3 and polyneuropathy often segregate in autosomal dominant families, those with more severe clinical findings typically arise *de novo*. Overall, most adults with isolated CFEOM3 have R262C or, less commonly, R62Q or A302T substitutions. Some children with isolated CFEOM3, however, harbor the D417N substitution and are at risk of developing a polyneuropathy in their teens or twenties. CFEOM3 with developmental delay, CC agenesis, and basal ganglia dysmorphisms in the absence of facial weakness may be predictive of the R380C substitution. Association of severe CFEOM3 with facial weakness, developmental delay, moderate to severe CC dysgenesis and likely a late-onset polyneuropathy predicts the E410K substitution, while the addition of finger contractures, basal ganglia dysmorphisms, and early onset polyneuropathy would suggest R262H or D417H substitutions.

Multiple findings suggest the mutations underlying the *TUBB3* syndromes primarily alter microtubule function in a dominant fashion, although we cannot rule out partial loss of function for some. First, recurrent missense mutations in the absence of truncating mutations are most consistent with altered rather than loss of protein function as a primary genetic etiology. Second, facial paralysis and progressive sensorimotor polyneuropathy occur only in those individuals harboring R262H, E410K, D417H/N, the four mutations that permit heterodimer formation and efficient microtubule incorporation, and have dominant effects

upon microtubule function by perturbing kinesin interactions in yeast. Third, among the four mutations that result in scant heterodimer formation, A302T and R380C have considerably more microtubule incorporation in mammalian cells and cause more severe phenotypes than R62Q and R262C. Finally, R262C and R262H result in relatively isolated CFEOM3 and a severe TUBB3 phenotype, respectively; these two substitutions are distinguished because R262H permits much more efficient heterodimer formation and microtubule incorporation than R262C both *in vitro* and in mammalian cells. Thus, more severe phenotypes and developmental disabilities that correlate with particular mutations might reflect a greater extent of mutant heterodimer incorporation and the specific nature of the dominant effect (i.e. dynamics, protein interactions).

Motor protein trafficking defects result in progressive axonal neuropathy

Progressive axonal neuropathies can result from inactivating mutations in kinesin and dynein accessory proteins, underscoring the vulnerability of motor neurons and peripheral axons to protein trafficking defects (Chevalier-Larsen and Holzbaur, 2006). The TUBB3 syndromes now demonstrate that tubulin mutations resulting in secondary motor protein transport defects can also cause axonal neuropathies. *TUBB3* expression is maintained at high levels only in the adult PNS (Jiang and Oblinger, 1992), supporting a role for TUBB3 in health and maintenance of peripheral motor and sensory axons. This role is in addition to the function of TUBB3 in cranial nerve development, and perturbations in protein trafficking caused by a subset of TUBB3 substitutions may also explain, in part, the cellular etiology of CFEOM3. Notably, recurrent dominant mutations in *KIF21A* result in CFEOM1 and, in rare families, CFEOM3 (Yamada et al., 2004). Our findings in mice suggest that mutations in *TUBB3* can diminish KIF21A-microtubule interactions, possibly accounting for oculomotor nerve axon guidance defects.

TUBB3 is required for proper axon guidance

Neuroimaging, clinical manifestations of cranial motor nerve misrouting, and the phenotypic analysis of a TUBB3 disease mouse model elucidate a critical role for TUBB3 in proper axon guidance. Throughout nervous system development, differentiating neurons require dynamic populations of microtubules in order to appropriately respond to growth and guidance cues (Gordon-Weeks, 2004; Kalil and Dent, 2005). Because TUBB3 is the most dynamic β -tubulin isotype and the only one with expression primarily restricted to the CNS and PNS (Katsetos et al., 2003), it has been hypothesized that the dynamic properties of TUBB3 could be required for specific developmental processes (Panda et al., 1994). We expand upon these earlier observations by demonstrating microtubule stability is increased in homozygous R262C mice, a finding that could result from the combined effects of TUBB3 heterodimer loss and the remaining mutant heterodimers. Dynamic changes could be exacerbated further by mutant heterodimers that diminish microtubule dynamics and incorporate at higher levels (R380C), resulting in more severe axon guidance phenotypes.

Tubulin isotypes have divergent cellular functions

Certain aspects of the TUBB3 syndromes, including CC dysgenesis and basal ganglia dysmorphisms, converge with those resulting from heterozygous missense mutations in *TUBA1A* and *TUBB2B* in humans (Jaglin et al., 2009; Keays et al., 2007). Each of these three tubulin isotypes are highly expressed in post-mitotic differentiating neurons and the phenotypic similarities suggest they have important overlapping functions (Coksaygan et al., 2006; Jaglin et al., 2009; Liu et al., 2007). However, the primary brain malformations resulting from mutations in *TUBA1A* and *TUBB2B* are lissencephaly, pachygyria, and/or grey matter heterotopias that result from cell migration defects. By contrast, humans and mice with TUBB3 substitutions do not show signs of cortical cell migration defects, and a recent study of *TUBA1A* mutation-negative subjects ascertained on the basis of agyria and

pachygyria failed to identify mutations in *TUBB3* (Poirier et al., 2007) and instead identified *TUBB2B* (Jaglin et al., 2009).

Remarkably, TUBB2B and TUBB3 are the major β -tubulin isotypes expressed in the nervous system and share 90% protein sequence homology, including all disease-associated amino acids. These isotypes differ, however, in the sequence of their C-terminal tails, dynamic behavior *in vitro*, and unique post-translational modifications (Banerjee et al., 1990; Khan and Luduena, 1996), suggesting that functional differences between these isotypes may account for phenotypic distinctions in humans and mice. Our results now greatly expand upon previous observations that different β -tubulin isotypes may have evolved in higher vertebrates to serve specific cellular functions (Luduena, 1993), and support a critical role for TUBB3 in axon guidance.

Experimental Procedures

Detailed experimental procedures can be found in Supplemental Data.

Clinical genetic studies

Probands were ascertained based on affection with CFEOM. Participants were enrolled by the Engle Laboratory at Children's Hospital Boston or by collaborating laboratories following appropriate Institutional Review Board approval and informed consent. Clinical data were obtained from participants and medical providers. Genetic linkage and mutation detection by direct sequencing and DHPLC were performed as previously described (Doherty et al., 1999; Miyake et al., 2008) and using NCBI reference sequences NM_006086 and NT_010542.

Magnetic Resonance Imaging

Diagnostic MRI scans were reviewed from participants with each TUBB3 substitution except D417H. Images are T1 (B-E, G, B', F'), T2 (A, F, H, J-N, A'-D', G', H'), Flair (I). Orbital MRI was performed as described previously (Demer et al., 2005).

Mouse histology, whole-mount neurofilament staining, and dissociated neuronal cultures

E18.5 embryonic brains on mixed 129/B6 and pure 129S6 backgrounds were fixed in 4% paraformaldehyde and embedded for cryo- or paraffin sectioning. 10–12 μ m sections were blocked with 5% normal goat/donkey serum and 0.1% Triton in PBS at room temperature for 1 hr, and incubated with primary antibody in 1% serum and 0.01% Triton at 4 C overnight. Secondary antibody was added at room temperature for 1 hr.

Microtubule repolymerization assay

E18 whole brains from WT, heterozygous, and homozygous mutant mice were homogenized in BRB80 buffer and centrifuged at 50,000G at 4 C for 30 minutes. 1mM GTP was added to supernatant and microtubules were polymerized for 30 minutes at 37 C. Samples were layered on a 30% sucrose cushion and centrifuged for 20 minutes at 37 C at 100,000g to pellet the microtubules.

Co-purification of kinesin with microtubules

E18 brains from WT and homozygous mutant mice were homogenized with a glass homogenizer in BRB80 buffer containing protease inhibitors and PMSF and incubated on ice for 20 minutes. A tubulin rich fraction was obtained by centrifuging the lysates at 4 C for 30 minutes at 50,000g. 1mM ATP, 1mM GTP, and 10 μ M taxol were added to the supernatants and incubated at 37 C for 30 minutes. Samples were then layered on top of a

30% sucrose cushion and centrifuged for 20 minutes at 37 C at 100,000g. Pellets were resuspended in SDS buffer and run on SDS NuPAGE 8–12% Bis-Tris gels (Invitrogen).

***In vitro* heterodimer formation and cycling**

1 μ g of plasmid DNA was added to 50 μ l of reticulocyte cocktail according to manufacturer's instructions (Promega TNT T7 Coupled Reticulocyte Lysate), and the reactions were incubated at 30°C for 90 minutes. Following incubation, the products were chased with 300ng bovine brain tubulin and 1mM MgCl₂ and GTP for 30 minutes at 37 C, and 2 μ l and 10 μ l from the overall reactions were run on SDS NuPAGE 8–12% Bis-Tris (Invitrogen) and NativePAGE 4–16% Bis-Tris Gels (Invitrogen), respectively. WT and mutant TUBB3 heterodimers were detected with a monoclonal V5 antibody (Invitrogen) against the C-terminal tag. Remaining products were cycled with bovine brain tubulin.

Mutation Modeling

Each TUBB3 substitution was plotted on the solved protein structure for the $\alpha\beta$ -tubulin heterodimer (pdb: 1JFF) using PyMOL software (1.1r1, <http://www.pymol.org>). Hydrogen bonds were predicted using the bond distance measurement function, and were also modeled using the Swiss-Pdb Viewer (DeepView). The protein model movie was created using PyMOL.

Yeast *in vivo* microtubule dynamics

Cells were seeded overnight in SD-complete media (0.67% yeast nitrogen base without amino acids, 5% glucose, 0.5% casamino acids) and allowed to grow at 24°C. The next morning, cells were reseeded and grown at 24°C to mid-log phase. 1 ml of cells were pelleted, resuspended in SD-complete media, imaged at room temperature (~26°C) on an Axio Image MI (Zeiss) scope with a 63 \times Plan Fluor 1.4 N.A. objective, and captured using a Coolsnap HQ camera (Photometrics). The typical acquisition protocol acquired five z-series fluorescent images at 0.75 μ m axial steps, and one differential interference contrast (DIC) image corresponding to the central fluorescent image. Time-lapse image series were acquired at 8 sec intervals.

Kip3p-3YFP and Kip2p-3YFP microtubule plus-end localization

Mutant and WT CFP-Tub1p-expressing cells containing either Kip3p-3YFP or Kip2p-3YFP were grown and imaged as described above in the *in vivo* microtubule dynamics section. Seven z-series images were merged into a single projection image (maximum) using deconvolution microscopy and the nearest neighbor algorithm function in Slidebook software (Intelligent Imaging Innovations, CO). In randomly selected fields, the plus-ends of all identifiable microtubules in multiple cells in all phases of the cell cycle were marked with a circle of equal radius, and the average plus-end intensity was then calculated using quantification software (Slidebook). At least two clones from WT and mutant strains were analyzed on at least two separate days, and net signal intensities from microtubule plus-ends and cell backgrounds were determined by averaging the values obtained from the total population on each day.

Supplementary Material

Refer to Web version on PubMed Central for supplementary material.

Acknowledgments

We thank the families for their participation; Michelle DeLisle and Carrie Wu for technical assistance, and members of the Engle lab for their thoughtful comments; A. Nurten Akarsu, Peter Kang, Lisa S Kearns, James

Hoekel, Marijean Miller, Marilyn Miller, Peter Roggenkämper, and Sandra Staffieri for pedigree referrals and/or clinical exam data. This work was supported by NIH R01 EY012498, R01 EY013583, HD18655 [ECE], F32 EY016306 [HB], R01 GM061345-08 [DP], and VA Research Funds [TDB]. ECE and DP are investigators of the Howard Hughes Medical Institute.

References

- Al-Bassam J, Ozer RS, Safer D, Halpain S, Milligan RA. MAP2 and tau bind longitudinally along the outer ridges of microtubule protofilaments. *J Cell Biol.* 2002; 157:1187–1196. [PubMed: 12082079]
- Banerjee A, Roach MC, Trcka P, Luduena RF. Increased microtubule assembly in bovine brain tubulin lacking the type III isotype of beta-tubulin. *J Biol Chem.* 1990; 265:1794–1799. [PubMed: 2404018]
- Carminati JL, Stearns T. Microtubules orient the mitotic spindle in yeast through dynein-dependent interactions with the cell cortex. *J Cell Biol.* 1997; 138:629–641. [PubMed: 9245791]
- Carvalho P, Gupta ML Jr, Hoyt MA, Pellman D. Cell cycle control of kinesin-mediated transport of Bik1 (CLIP-170) regulates microtubule stability and dynein activation. *Dev Cell.* 2004; 6:815–829. [PubMed: 15177030]
- Chevalier-Larsen E, Holzbaaur EL. Axonal transport and neurodegenerative disease. *Biochim Biophys Acta.* 2006; 1762:1094–1108. [PubMed: 16730956]
- Cleveland DW, Kirschner MW, Cowan NJ. Isolation of separate mRNAs for alpha- and beta-tubulin and characterization of the corresponding in vitro translation products. *Cell.* 1978; 15:1021–1031. [PubMed: 728983]
- Coksaygan T, Magnus T, Cai J, Mughal M, Lepore A, Xue H, Fischer I, Rao MS. Neurogenesis in Talpha-1 tubulin transgenic mice during development and after injury. *Exp Neurol.* 2006; 197:475–485. [PubMed: 16336967]
- Demer JL, Clark RA, Engle EC. Magnetic resonance imaging evidence for widespread orbital dysinnervation in congenital fibrosis of extraocular muscles due to mutations in KIF21A. *Invest Ophthalmol Vis Sci.* 2005; 46:530–539. [PubMed: 15671279]
- DeZwaan TM, Ellingson E, Pellman D, Roof DM. Kinesin-related KIP3 of *Saccharomyces cerevisiae* is required for a distinct step in nuclear migration. *J Cell Biol.* 1997; 138:1023–1040. [PubMed: 9281581]
- Doherty EJ, Macy ME, Wang SM, Dykeman CP, Melanson MT, Engle EC. CFEOM3: a new extraocular congenital fibrosis syndrome that maps to 16q24.2-q24.3. *Invest Ophthalmol Vis Sci.* 1999; 40:1687–1694. [PubMed: 10393037]
- Gordon-Weeks PR. Microtubules and growth cone function. *J Neurobiol.* 2004; 58:70–83. [PubMed: 14598371]
- Gupta ML Jr, Carvalho P, Roof DM, Pellman D. Plus end-specific depolymerase activity of Kip3, a kinesin-8 protein, explains its role in positioning the yeast mitotic spindle. *Nat Cell Biol.* 2006; 8:913–923. [PubMed: 16906148]
- Jaglin XH, Poirier K, Saillour Y, Buhler E, Tian G, Bahi-Buisson N, Fallet-Bianco C, Phan-Dinh-Tuy F, Kong XP, Bomont P, et al. Mutations in the beta-tubulin gene TUBB2B result in asymmetrical polymicrogyria. *Nat Genet.* 2009; 41:746–752. [PubMed: 19465910]
- Jiang YQ, Oblinger MM. Differential regulation of beta III and other tubulin genes during peripheral and central neuron development. *J Cell Sci.* 1992; 103(Pt 3):643–651. [PubMed: 1478962]
- Joshi HC, Cleveland DW. Diversity among tubulin subunits: toward what functional end? *Cell Motil Cytoskeleton.* 1990; 16:159–163. [PubMed: 2194680]
- Kalil K, Dent EW. Touch and go: guidance cues signal to the growth cone cytoskeleton. *Curr Opin Neurobiol.* 2005; 15:521–526. [PubMed: 16143510]
- Katsetos CD, Legido A, Perentes E, Mork SJ. Class III beta-tubulin isotype: a key cytoskeletal protein at the crossroads of developmental neurobiology and tumor neuropathology. *J Child Neurol.* 2003; 18:851–866. discussion 867. [PubMed: 14736079]
- Keays DA, Tian G, Poirier K, Huang GJ, Siebold C, Cleak J, Oliver PL, Fray M, Harvey RJ, Molnar Z, et al. Mutations in alpha-tubulin cause abnormal neuronal migration in mice and lissencephaly in humans. *Cell.* 2007; 128:45–57. [PubMed: 17218254]

- Khan IA, Luduena RF. Phosphorylation of beta III-tubulin. *Biochemistry (Mosc)*. 1996; 35:3704–3711.
- Lewis SA, Tian G, Vainberg IE, Cowan NJ. Chaperonin-mediated folding of actin and tubulin. *J Cell Biol*. 1996; 132:1–4. [PubMed: 8567715]
- Li H, DeRosier DJ, Nicholson WV, Nogales E, Downing KH. Microtubule structure at 8 Å resolution. *Structure*. 2002; 10:1317–1328. [PubMed: 12377118]
- Liu L, Geisert EE, Frankfurter A, Spano AJ, Jiang CX, Yue J, Dragatsis I, Goldowitz D. A transgenic mouse Class-III beta tubulin reporter using yellow fluorescent protein. *Genesis*. 2007; 45:560–569. [PubMed: 17868115]
- Lopata MA, Cleveland DW. In vivo microtubules are copolymers of available beta-tubulin isotypes: localization of each of six vertebrate beta-tubulin isotypes using polyclonal antibodies elicited by synthetic peptide antigens. *J Cell Biol*. 1987; 105:1707–1720. [PubMed: 3312237]
- Lowe J, Li H, Downing KH, Nogales E. Refined structure of alpha beta-tubulin at 3.5 Å resolution. *J Mol Biol*. 2001; 313:1045–1057. [PubMed: 11700061]
- Luduena RF. Are tubulin isotypes functionally significant. *Mol Biol Cell*. 1993; 4:445–457. [PubMed: 8334301]
- Mackey DA, Chan WM, Chan C, Gillies WE, Brooks AM, O’Day J, Engle EC. Congenital fibrosis of the vertically acting extraocular muscles maps to the FEOM3 locus. *Hum Genet*. 2002; 110:510–512. [PubMed: 12073023]
- Miyake N, Chilton J, Psatha M, Cheng L, Andrews C, Chan WM, Law K, Crosier M, Lindsay S, Cheung M, et al. Human CHN1 mutations hyperactivate alpha2-chimaerin and cause Duane’s retraction syndrome. *Science*. 2008; 321:839–843. [PubMed: 18653847]
- Nogales E, Wang HW. Structural intermediates in microtubule assembly and disassembly: how and why? *Curr Opin Cell Biol*. 2006; 18:179–184. [PubMed: 16495041]
- Panda D, Miller HP, Banerjee A, Luduena RF, Wilson L. Microtubule dynamics in vitro are regulated by the tubulin isotype composition. *Proc Natl Acad Sci U S A*. 1994; 91:11358–11362. [PubMed: 7972064]
- Poirier K, Keays DA, Francis F, Saillour Y, Bahi N, Manouvrier S, Fallet-Bianco C, Pasquier L, Toutain A, Tuy FP, et al. Large spectrum of lissencephaly and pachygyria phenotypes resulting from de novo missense mutations in tubulin alpha 1A (TUBA1A). *Hum Mutat*. 2007; 28:1055–1064. [PubMed: 17584854]
- Reijo RA, Cooper EM, Beagle GJ, Huffaker TC. Systematic mutational analysis of the yeast beta-tubulin gene. *Mol Biol Cell*. 1994; 5:29–43. [PubMed: 8186463]
- Uchimura S, Oguchi Y, Katsuki M, Usui T, Osada H, Nikawa J, Ishiwata S, Muto E. Identification of a strong binding site for kinesin on the microtubule using mutant analysis of tubulin. *EMBO J*. 2006; 25:5932–5941. [PubMed: 17124495]
- Webster DR, Gundersen GG, Bulinski JC, Borisy GG. Differential turnover of tyrosinated and detyrosinated microtubules. *Proc Natl Acad Sci U S A*. 1987; 84:9040–9044. [PubMed: 3321065]
- Yamada K, Andrews C, Chan WM, McKeown CA, Magli A, De Berardinis T, Loewenstein A, Lazar M, O’Keefe M, Letson R, et al. Heterozygous mutations of the kinesin KIF21A in congenital fibrosis of the extraocular muscles type 1 (CFEOM1). *Nat Genet*. 2003; 35:318–321. [PubMed: 14595441]
- Yamada K, Chan WM, Andrews C, Bosley TM, Sener EC, Zwaan JT, Mullaney PB, Ozturk BT, Akarsu AN, Sabol LJ, et al. Identification of KIF21A Mutations as a Rare Cause of Congenital Fibrosis of the Extraocular Muscles Type 3 (CFEOM3). *Invest Ophthalmol Vis Sci*. 2004; 45:2218–2223. [PubMed: 15223798]



Figure 1. Clinical spectrum and orbital imaging of the TUBB3 syndromes

(A–I) Study participant photographs. R262C can cause bilateral ptosis and severe CFEOM3 with the resting position of both eyes infraducted and abducted (A), moderate CFEOM3 that can be unilateral (B), and mild CFEOM3 (not shown). A similar spectrum is seen with D417N; severe CFEOM3 is shown in (E). A302T (C) and R380C (D) cause moderate to severe CFEOM3. Participants in (A–E) have full facial movements. The axonal neuropathy in the participant with D417N (E) results in atrophy of the intrinsic foot muscles and a high arch (F). E410K (G) and R262H (H) result in severe CFEOM3 and facial weakness, and R262H also results in congenital ulnar deviation of the hand with joint contractures of the thumbs and fingers (I). (J–L) MRI of the brainstem at the level of the oculomotor nerve (J) and orbital contents posterior to the globe (K) in a participant with predominantly left-sided CFEOM3 and a D417N substitution. Note unilateral hypoplasia of the left oculomotor nerve (J, arrow) and the atrophy of the levator palpebrae superioris (LPS), superior rectus (SR), and medial rectus (MR) muscles in (K). The inferior rectus (IR), lateral rectus (LR), and superior oblique (SO) muscles appear normal. (L) Control orbital MRI for comparison. (ON) denotes optic nerve.

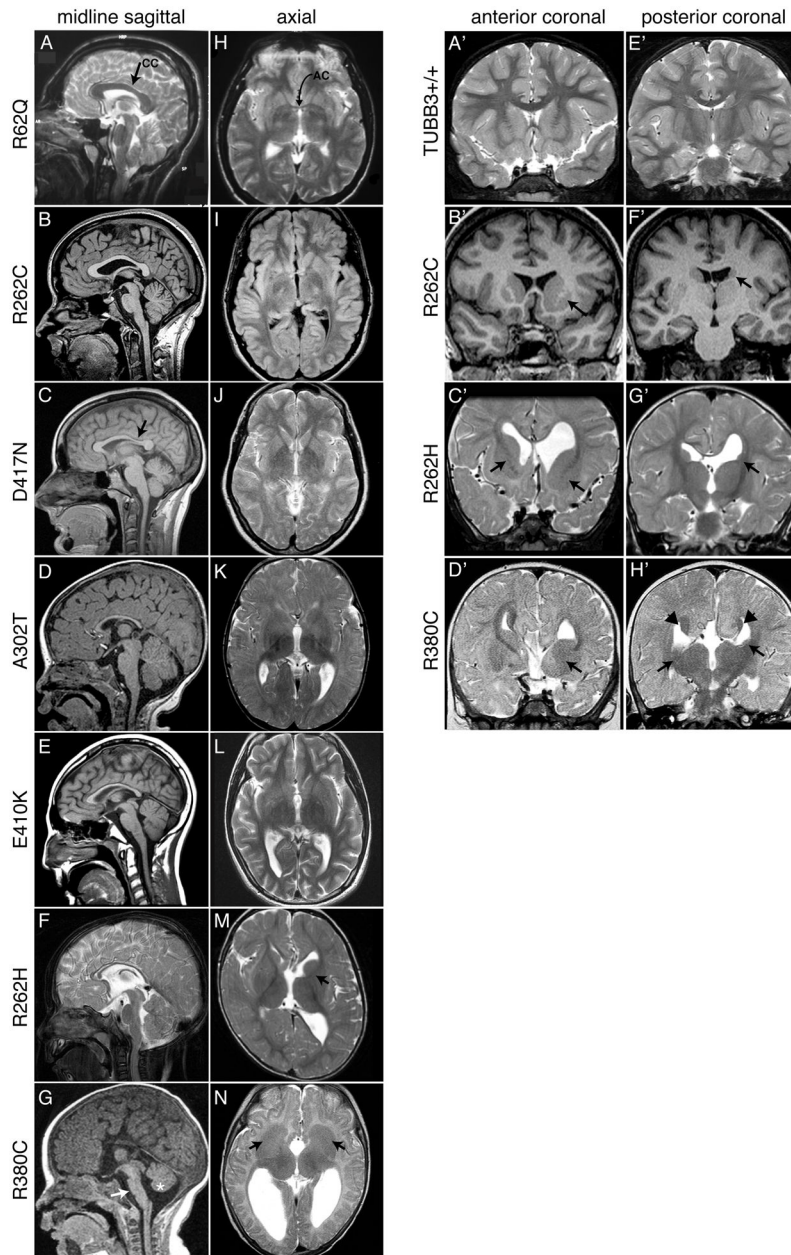


Figure 2. Spectrum of human brain malformations correlate with specific *TUBB3* mutations (A–G) Midline sagittal MRI showing the spectrum of corpus callosum (CC) dysgenesis; corresponding amino acid substitutions are noted to the left. R62Q (A) and most R262C (B) participants have normal CC development, whereas D417N subjects have hypoplasia of the posterior body (C, arrow). Subjects with A302T, E410K, and R262H have diffuse CC hypoplasia (D–F). (G) Both R380C siblings have CC agenesis, and brainstem (arrow) and mild vermian hypoplasia (asterisk). (H–N) Axial MRI from the same patient scans showing the spectrum of anterior commissure (AC) dysgenesis and overall loss of white matter compared to the normal R62Q scan (H, arrow indicates AC). (I–L) Subjects have hypoplastic AC. R262H (M) and R380C (N) patient scans show AC agenesis and dysmorphic basal ganglia. The anterior limb of the left internal capsule is hypoplastic in R262H (M, arrow), while there is lack of clear separation between the caudate and putamen

and bilateral hypoplasia of the anterior limbs of the internal capsule with R380C (N, arrows). (A'-H') Anterior (A'-D') and posterior (E'-H') coronal sections showing the spectrum of basal ganglia dysmorphisms present in individuals with R262C, R262H, and R380C substitutions (Figure 3A'-H'). (A'-D') Compared to a *TUBB3*^{+/+} scan (A'), R262C reveals asymmetric basal ganglia with enlargement of the left caudate head and putamen (B' arrow). (C') The twin of the R262H patient in (F, M) has dysgenesis of the left and right anterior limbs of the internal capsule (C' arrows), apparent fusion of an enlarged left caudate head with the putamen, and dilatation of the left and right anterior horn of the lateral ventricle. (D') The older sibling of the patient scanned in (G, N) harboring an R380C substitution has hypoplasia of the anterior limb of the internal capsule (D' arrow) and fusion of the left caudate head and underlying putamen. (E'-H') Coronal MRI at the level of the caudate body and lateral ventricles is normal in (E'). R262C and R262H subjects have hypoplasia of the left caudate body (F', G', arrows) and tail, and the R262H patient has dilatation of the left lateral ventricle. (H') The R380C patient has bilateral hypoplasia of the caudate body and tail, with Probst bundles of callosal axons that line the bodies of the lateral ventricles (arrow heads).

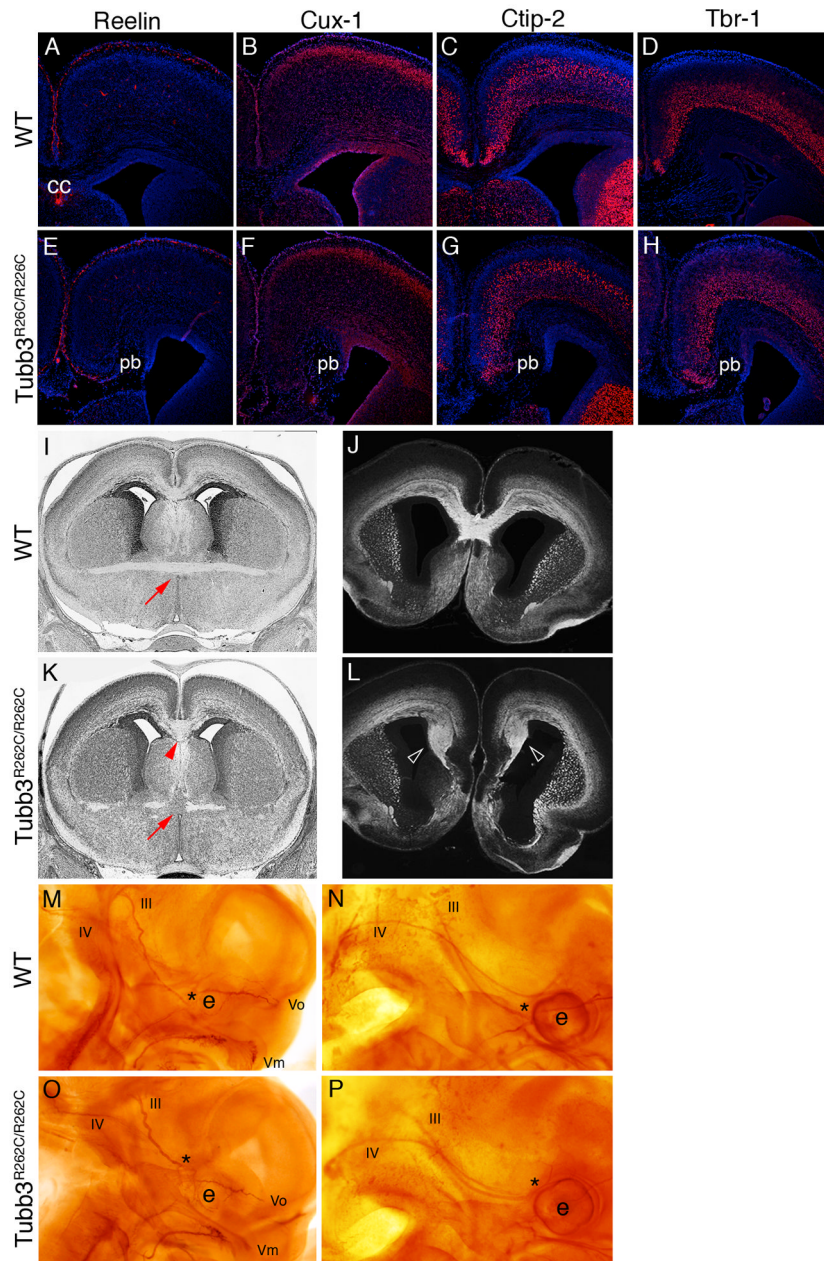


Figure 3. TUBB3^{R262C/R262C} mice have normal cortical layering but show defects in axon guidance

(A–D, n=5) WT and TUBB3^{R262C/R262C} (E–H, n=5) E18.5 coronal sections immunostained with markers specific for cortical layers show that the cortex has developed properly. Mild midline changes result from large Probst bundles (pb), comprised of stalled commissural axons adjacent to the midline. (I and K) Coronal sections from E18.5 WT (I, n=4) and TUBB3^{R262C/R262C} (K, n=5) embryos show that the anterior commissure (red arrow) appears broken and fails to cross the midline, while the CC has crossed but is abnormally thick (red arrowhead) in the mutant. (J and L) E18.5 coronal sections from embryos immunostained with the axonal marker L1 show Probst bundles in a TUBB3^{R262C/R262C} (L, arrowheads) mutant compared to WT (J). (M–P) Whole-mount neurofilament staining of E11.5–12 WT (M, N; n=13) and TUBB3^{R262C/R262C} (O, P; n=6) embryos. Mutant

oculomotor (III) and trochlear (IV) nerves, as well the maxillary (Vm) and ophthalmic (Vo) divisions of the trigeminal nerve are stalled at E11.5 (O) compared to WT (M). At E12, the mutant oculomotor nerve follows an aberrant course adjacent to the trochlear nerve (P) compared to WT (N,). CC = corpus callosum; e = eye; asterisk (*)= distal tip of oculomotor nerve.

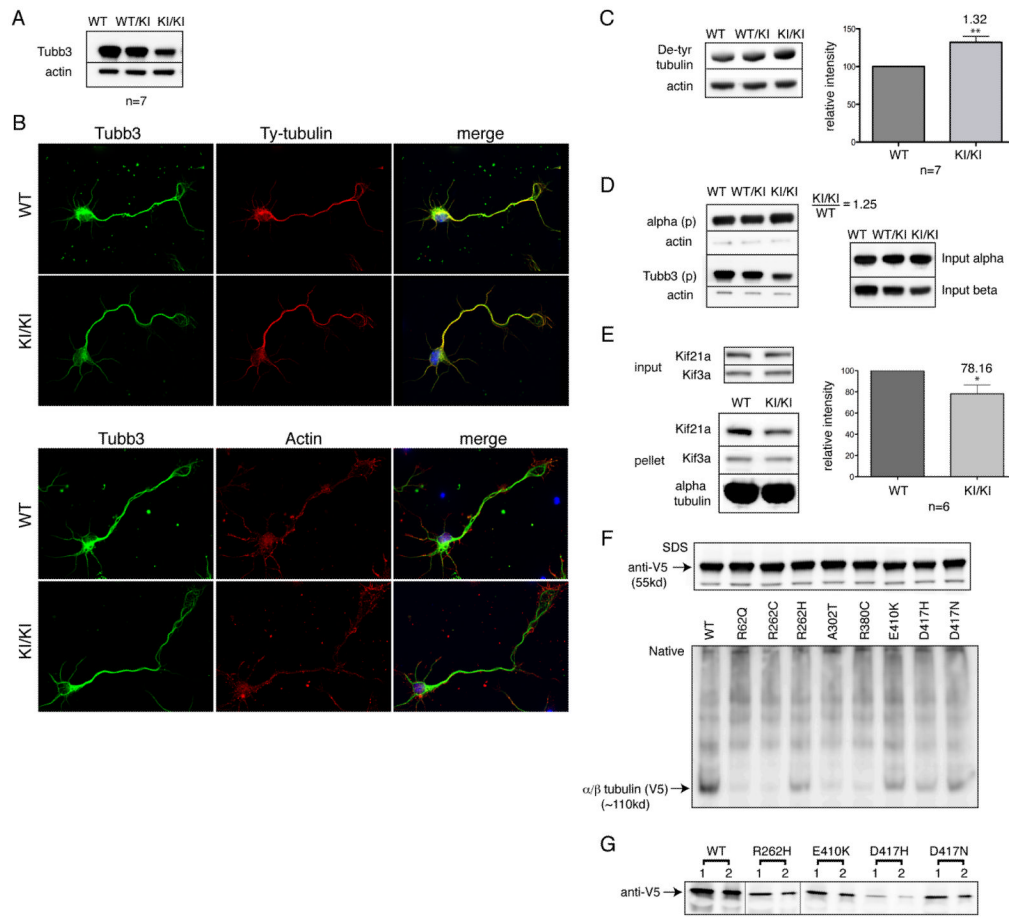


Figure 4. TUBB3^{R262C/R262C} mice have low TUBB3 protein levels, altered microtubule stability, and decreased Kif21a interactions

(A) TUBB3 protein levels are reduced in TUBB3^{+/R262C} (WT/KI) and TUBB3^{R262C/R262C} (KI/KI) vs. WT mice. (B) TUBB3 R262C heterodimers incorporate into microtubules throughout cell bodies, neurites, and growth cones of dissociated cortical neurons as seen by co-localization with tyrosinated -tubulin and actin. Variable reductions in TUBB3 staining intensity are noted between WT and mutant neurons. (C) Levels of de-tyrosinated -tubulin are increased in brain lysates from mutant versus WT mice. (D) Brain lysates from TUBB3^{R262C/R262C} mice show increased microtubule polymerization at steady-state levels despite lower levels of β -tubulin. Mutant TUBB3 is detected in the pellets (p). (E) Levels of Kif21a are reduced on TUBB3^{R262C/R262C} mutant microtubules polymerized *in vitro* from brain lysates and incubated with ATP, whereas levels of Kif3a remain constant. (F) *In vitro* transcription and translation of WT and TUBB3 mutant heterodimers in rabbit reticulocyte lysate. Products analyzed by SDS (top) and non-denaturing (native, bottom) gel electrophoresis and stained with an anti-V5 antibody against the C-terminal tag demonstrate that although transcription and translation are not affected by the mutations, there can be significant and variable decreases in the yield of native heterodimers. (G) Synthesized WT, R262H, E410K, and D417H/N heterodimers cycle with native bovine tubulin at equivalent efficiency; vertical lines denote removed empty lanes. * $P < 0.05$, ** $P < 0.001$.

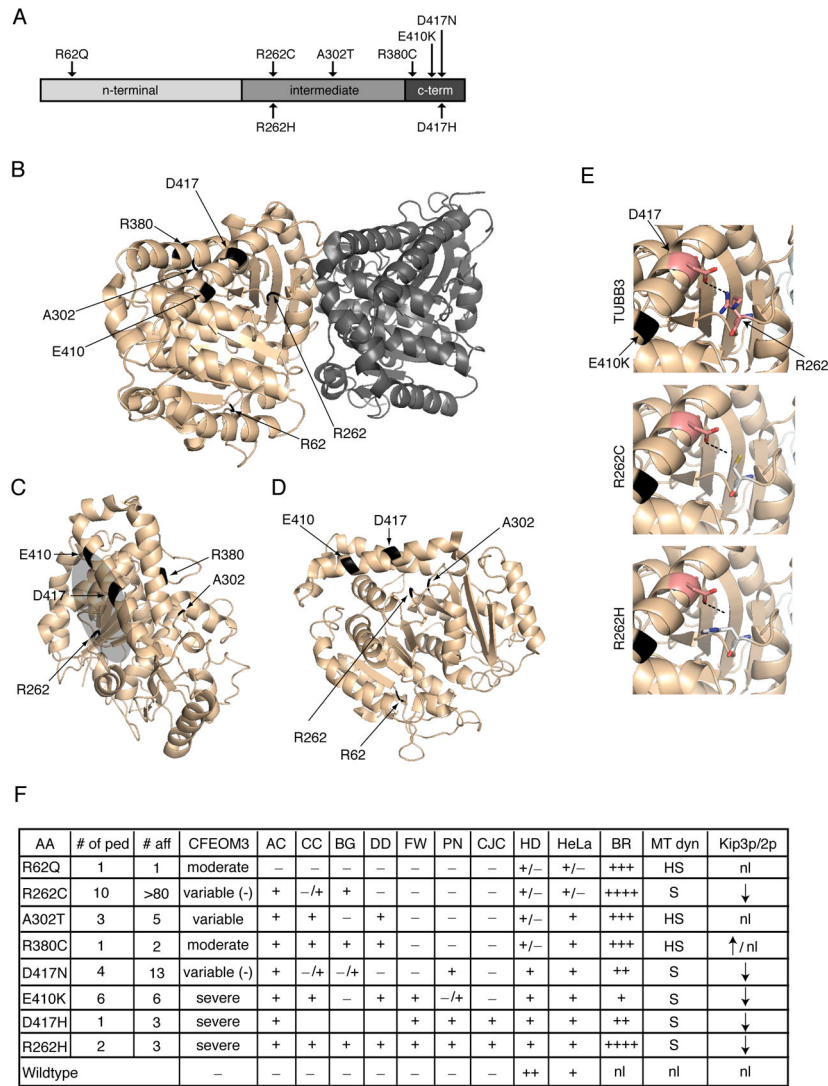


Figure 5. TUBB3 amino acid substitutions and phenotype-genotype-function correlations
 (A) Schematic of the TUBB3 protein; arrows indicate the location of each TUBB3 amino acid substitution. (B) Structure of the $\alpha\beta$ -tubulin heterodimer from a rotated side view (pdb: 1JFF). α -tubulin is dark-shaded on right, and the arrows on the left point to each mutant residue, depicted in black, on β -tubulin. (C) Outside view of β -tubulin depicting each mutant residue in black with the exception of R62Q, which cannot be seen. The area proposed for motor protein interactions is depicted as a shaded grey oval. Residues R380, E410 and D417 are found in helices H11 and H12, respectively, on the external surface of β -tubulin. R262, found in the loop between helix H8 and strand 7, and A302, found in the loop following helix H9, are positioned laterally and below to helices H12 and H11, respectively. (D) Side interior view of β -tubulin showing the location of each mutant residue in black, with the exception of R380C, which is occluded by D417. R62 is positioned in the H1-S2 loop (N-loop) that forms lateral contacts with the M-loop of adjacent protofilaments. (E, top) Magnified image of β -tubulin depicting the putative hydrogen bond between the arginine side chain of R262 and the carbonyl oxygen of D417, both of which are shown in a stick representation. (E, middle and bottom) Both the R262C and R262H substitutions are predicted to break the hydrogen bond. (F) Phenotype-genotype and summary of functional

data. AA = amino acid substitution; # ped = number of pedigrees; # aff = number of affected individuals; AC = anterior commissure hypoplasia; CC = corpus callosum hypoplasia; BG = basal ganglia dysgenesis; DD = developmental delay; FW = facial weakness; PN = progressive axonal sensorimotor polyneuropathy; CJC = congenital joint contractures; HD = heterodimer formation; HeLa = HeLa cell incorporation; MT dyn = microtubule dynamics (HS = highly stable, S = stable); Kip3p/2p = Kip3p and Kip2p microtubule plus-end accumulation (↓ decreased, ↑ increased). + denotes present; - denotes absent; -/+ denotes that only a subset of subjects have the feature and/or the findings are mild; variable (-) denotes rare participants with the substitution without CFEOM3.

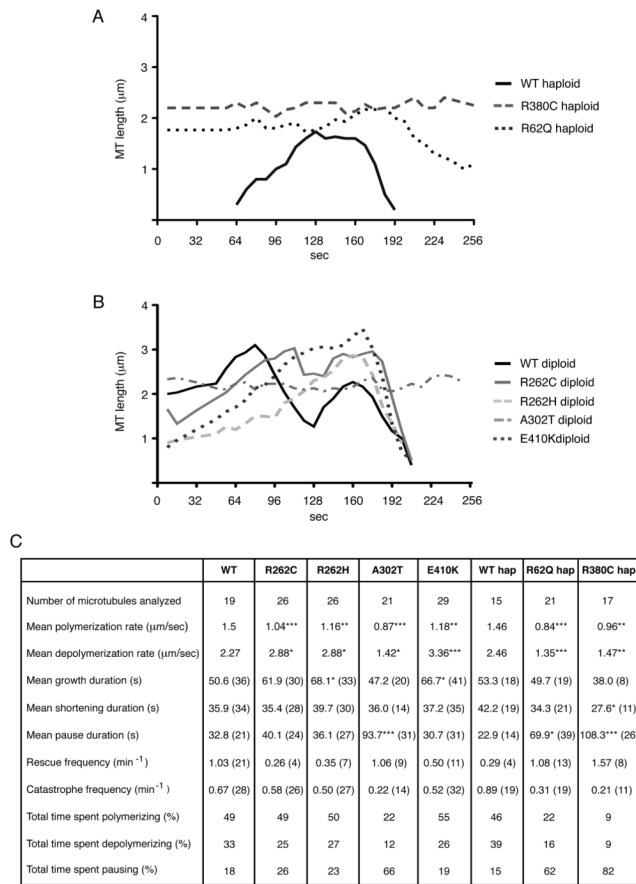


Figure 6. TUBB3 disease amino acid substitutions results in changes to microtubule dynamic instability

(A, B) 4-D life-time plots depicting the lengths of microtubules (Y axis) over time (X axis) in G1 cells from (A) haploid WT and *TUB2* mutants and (B) heterozygous diploid WT and *TUB2* mutants demonstrate that Tub2p substitutions perturb microtubule dynamic instability. For WT and each mutation, one microtubule representing data from the collective analysis has been selected and plotted. (C) Summary table of individual dynamic instability parameters. Number of events is listed in parentheses. * $P < 0.05$, ** $P < 0.001$, *** $P < 0.0001$.

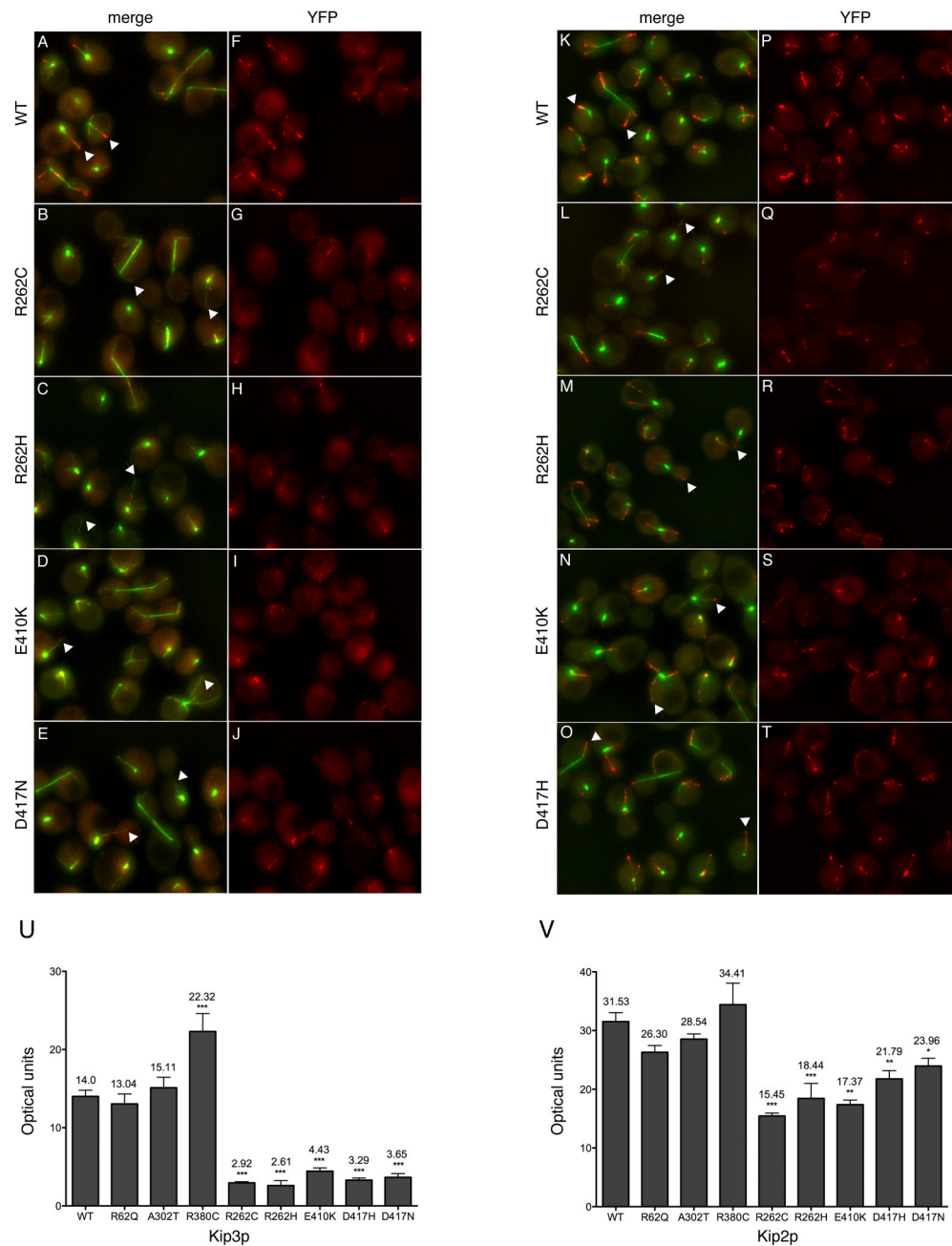


Figure 7. Kip3p and Kip2p levels are reduced at the plus-ends of mutant microtubules
 Merged z-stack images showing the levels of Kip3p-3YFP (A–E, red) and Kip2p-3YFP (K–O, red) on WT and mutant microtubules labeled with CFP-Tub1p (α -tubulin, green) in budding yeast. Corresponding Kip3p (F–J) and Kip2p (P–T) YFP channels with signal intensities adjusted equally for WT and each *TUB2* mutant are provided for comparison. In WT cells, Kip3p-3YFP (A, F) and Kip2p-3YFP (K, P) are speckled along the length and accumulate at the plus-ends of growing microtubules labeled by white arrows. In contrast, mutant R262C (B), R262H (C), E410K (D), and D417N (E) cells all have a significant reduction of Kip3p-3YFP along the length and plus-ends of microtubules (white-arrows), and Kip2p-3YFP is speckled along the length but reduced or absent on microtubule plus-

ends (white-arrows) in R262C (L), R262H (M), E410K (N), and D417H (O) cells. Graphs depicting the overall mean levels of Kip3p-YFP (U) and Kip2p-3YFP (V) on microtubule plus-ends in WT and mutant cells. * $P < 0.05$, ** $P < 0.001$, *** $P < 0.0001$.